Universidad de Alcalá
BIBLIOTECA

Document downloaded from the institutional repository of the University of Alcala: http://dspace.uah.es/dspace/

This is a postprint version of the following published document:

Monteagudo-Lerma, L., Naranjo, F.B., Valdueza Felip, S., Jiménez-Rodríguez, M., Monroy, E., Postigo, P.A., Corredera, P., González-Herráez, M., 2016, "III-nitride-based waveguides for ultrafast all-optical signal processing at 1.55 μm", Physica Status Solidi (A), Applications and Materials Science, 213 (5), pp. 1269-1275.

Available at http://dx.doi.org/10.1002/pssa.201532810

(Article begins on next page)

This work is licensed under a

Creative Commons Attribution-NonCommercial-NoDerivatives 4.0 International License.

III-nitride-based waveguides for ultrafast all-optical signal processing at 1.55 μm

Laura Monteagudo-Lerma[*,1], Fernando B. Naranjo[1], Sirona Valdueza-Felip[1], Marco Jiménez-Rodríguez[1], Eva Monroy[2,3], Pablo A. Postigo[3], Pedro Corredera[4], and Miguel González-Herráez[1]

[1] GRIFO, Departamento de Electrónica, Universidad de Alcalá, Ctra. Madrid-Barcelona km. 33.6, 28871 Alcalá de Henares, Madrid, Spain
[2] University Grenoble-Alpes, 38000 Grenoble, France
[3] CEA, INAC-SP2M, 17 av. des Martyrs, 38000 Grenoble, France
[4] Instituto de Microelectrónica de Madrid, CSIC, 28760 Tres Cantos, Madrid, Spain
[5] Instituto de Óptica, CSIC, Serrano 121, 28006 Madrid, Spain

Received ZZZ, revised ZZZ, accepted ZZZ
Published online ZZZ (Dates will be provided by the publisher.)

Keywords All-optical signal processing, III-nitrides, nonlinear optics, optical waveguides.

* Corresponding author: e-mail laura.monteagudo@depeca.uah.es, Phone: +34 91885 6913

We present an overview of the recently developed III-nitride-based optical waveguides for application in ultrafast signal processing at telecom wavelengths. We focus on different active and passive optical devices for further implementation within all-optical integrated circuits. Optical waveguides based on GaN/AlN quantum dots have been demonstrated to act as saturable absorbers requiring ~3 pJ of input pulse energy to reach +3 dB transmittance contrast for TM-polarized light. On the contrary, sputtered-InN-based devices show –3 dB transmittance contrast associated to two-photon absorption for input pulse energies of ~1 pJ, making them suitable to act as highly-efficient reverse saturable absorbers. Finally, the passive optical nature of waveguides based on sputtered AlN at 1.55 μm makes them suitable for further connections between different III-nitride-based active devices..

1 Introduction The evolution from electronic integrated circuits to photonic integrated circuits (PICs) is one of the most important challenges in the development of telecommunication networks. Current speed limitation is imposed by the optical-to-electrical-to-optical (OEO) conversions in each node of the system. To overcome this limitation, there are efforts to implement the whole data transmission and switching processes in the optical domain, in order to relegate OEO conversions to the edges of the network. In addition to higher speed, the concentration of multiple all-optical functions within a PIC should provide a significant reduction of cost, space, and power requirements, as well as a reliability improvement. Such integrated system would find a broad range of applications in the domain of optical communications, sensing, biophotonics, spectroscopy, etc.

Multi-terabit optical time division multiplexing networks require semiconductor all-optical switches and wavelength converters operating at room temperature. These devices should be characterized by ultrafast response capable of sustaining high repetition rates with low switching energy and high contrast ratio. There is a particular interest in the development of devices for the C-band of optical fibers, where erbium-doped fiber amplifiers are widely available. The required features lead to consider the use of resonant nonlinearities for the applications envisaged [1].

Si-based and InP-technologies have been widely used for operation at telecommunication wavelengths [2]. The technology based on Si present advantages in terms of low-cost production, CMOS compatibility, and the good waveguiding conditions provided by the high refractive index contrast between Si and SiO_2. On the other hand, the InP platform has been largely developed including optical functions such as emission, detection, wavelength multiplexing and demultiplexing, switching, etc. [3]. However, both silicon and InP technologies present operation speeds quite lower than the aimed data transmission rates per channel above 1 Tbps for all-optical signal processing. Particularly, Si bandwidth is limited up to ~40 Gbps per wavelength due to free carrier absorption

(FCA) generated via two-photon absorption (TPA) [4], whereas InP can reach data transmission rates up to ~50 Gbps per channel [5], being limited by the recovery time of the related electronic transition.

A promising alternative is the implementation of a PIC based on III-nitride semiconductors (GaN, AlN, InN, and their ternary alloys), since the asymmetry of their crystalline structure favors nonlinear phenomena. III-nitrides present several advantages: (i) their capability of tuning its direct optical band gap to make it resonant with the desired operation wavelength, (ii) their high thermal and chemical stability making them suitable for high-power nonlinear optical applications [6], and (iii) their better coupling with optical fibers thanks to the lower refractive index contrast compared to Si or InP.

In a III-nitride all-optical technology, passive optical waveguides (WGs) can be implemented by using AlN and/or GaN materials, since they are transparent in the 0.36−6.7 μm range. In the nonlinear regime, various approaches can be considered. A first strategy consists on using electronic transitions between confined states in the conduction band of GaN/AlN nanostructures (intraband transitions) [7]. Such transitions are subject to polarization selection rules: they are only allowed by interaction with light containing an electric field component parallel to the direction of confinement. Furthermore, the large conduction band offset in the GaN/AlN system (1.8 eV [8]) allows the tunning of the band gap of the intraband transition to 1.55 μm by controlling the size of the nanostructures. This material system presents intraband relaxation times below 400 fs at the C-band [9][14], making them suitable for ultrafast all-optical devices. On the other hand, the quantum confinement in nanostructures based on GaN/AlN such as quantum dots (QDs) and quantum wells (QWs) induces a resonant enhancement of the nonlinearities within the GaN/AlN system, demonstrated by third-order nonlinear susceptibility measurements [9],[12].

A second strategy is based on the use of InN grown by molecular-beam epitaxy (MBE), which presents a room temperature direct optical band gap of ~0.64 eV (~1.94 μm). Previous nonlinear optical measurements of InN films and InN/InGaN multi-QWs at 1.55 μm have been reported in refs. [15],[16]. These structures present interband relaxation times in the range of tens of ps [17].

Finally, a third low-cost approach consists on the use of RF-sputtered nanocrystalline InN, which presents RT direct band gap of ~1.7 eV (~730 nm). The nonlinear TPA was evaluated at 1.55 μm by Valdueza-Felip *et al.* [18], showing a recovery time of 380 fs.

In this work, we report the fabrication of three different WG architectures based on III-nitrides on sapphire platform for application in all-optical integrated circuits at 1.55 μm: (i) GaN WGs incorporating GaN/AlN QDs to operate as ultrafast saturable absorbers [19] (ii) nanocrystalline InN WGs grown by RF sputtering to operate as low-cost ultrafast reverse saturable absorbers [20] and (iii) passive AlN WGs deposited by RF sputtering to act as low-cost passive interconnectors.

2 Waveguide optical design The design of the WG was carried out taking into account both optical and electrical considerations. Optical modes propagating through the WG were calculated at $\lambda_0 = 1.55$ μm by using a commercial mode solver, assuming 1.746, 2.120, 2.280 and 2.317 as the linear refractive indices for sapphire, AlN, InN and GaN, respectively. The electronic features of the GaN/AlN heterostructures were modeled using the Nextnano3 8-band k.p Schrödinger-Poisson solver [21] with the material parameters described in ref. [22].

The main parameters taken into account to design the WG structure are: (i) the guiding layer thickness, (ii) the ridge width (w), and (iii) the etching depth (h), as displayed in Fig. 1 (right). The guiding layer thickness and the ridge width were optimized to attain modal guiding for WGs with the minimum ridge width affordable with the optical lithography used allowing single mode propagation along the device length (L). The etching depth was defined as short as possible to minimize optical losses due to modal guiding through the slab while maintaining the highest light confinement through single mode behavior.

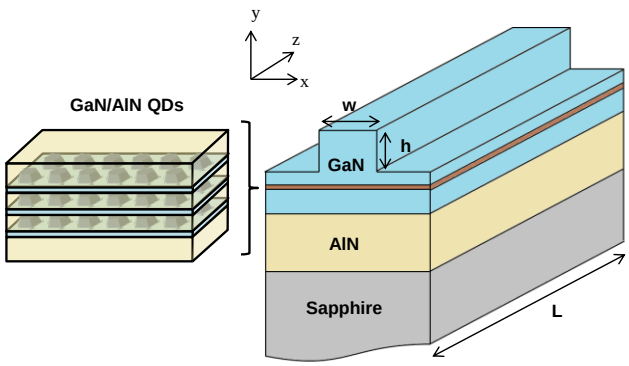

Figure 1 Scheme of the WG with GaN/AlN QDs as an active region with *w* the ridge width, *h* the etching depth and *L* the WG length.

3 Experimental setup Optical transmittance measurements were performed to characterize the linear and nonlinear behavior of the WGs at telecom wavelengths by using the experimental setup shown in Fig. 2 and widely described in ref. [19]. The propagation of light with transverse-electric (TE) and transverse-magnetic (TM) polarization was experimentally examined in all the cases.

Both propagation and coupling losses were estimated through the cutback method [23] at low incident optical power conditions.

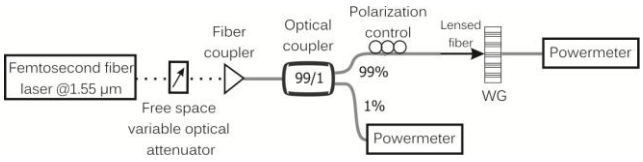

Figure 2 Scheme of the experimental setup used for the linear and nonlinear characterization of the WGs under study.

It has to be noticed that the term incident is referred to the light without taking into account the coupling losses at the input facet of the waveguiding devices. Contrarily, the term input already accounts for these losses.

4 III-nitride optical waveguides

4.1 GaN/AlN QD-based waveguides All-optical switching can be achieved through absorption saturation of the electronic transition by an intense control pulse, as originally demonstrated at long infrared wavelengths using GaAs/AlGaAs structures [24]. In the case of GaN/AlN heterostructures, the nonlinear behavior is obtained by intraband absorption saturation. Control switching energies of 38 pJ for reaching +10 dB optical transmittance contrast have been reported in ref. [25] for WGs containing GaN/AlN QWs in the active region. Studies on the nonlinear properties of GaN/AlN QD structures pointed out a five-fold increase of their third-order nonlinear susceptibility compared to their QWs counterparts, as a result of the higher carrier confinement in the QDs [9], which makes interesting the use of QDs instead of QWs as active elements.

In this section we report the electrical and optical requirements, growth, fabrication and optical characterization of WGs based on GaN/AlN QDs, designed to work as saturable absorbers for all-optical switching at 1.55 µm. Transmittance contrasts of +3 dB and +10 dB are obtained for 3 pJ and 8 pJ input pulse energies, respectively.

4.1.1 Optical and electrical design The sample under consideration consists of 3 periods of GaN/AlN QDs embedded in a guiding structure based on a GaN layer deposited on a 1.1-µm-thick AlN-on-sapphire template, as schemed in Fig. 1. Simulations indicate that a GaN guiding layer with a thickness of 600 nm grants single mode propagation for ridge widths affordable with optical lithography (~2 µm) regardless of the ridge etching depth. Single mode propagation reduces the coupling losses between the optical fiber and the WG, and the propagation losses thanks to the improved optical mode confinement. In addition, this modal confinement is highly required for nonlinear optics, increasing the optical power density propagating through the device. According to the optical simulations reported in ref. [19], 2-µm-wide WGs are single mode for WG lengths in the range below 2 mm. On the other hand, the AlN-sapphire substrate allows an adequate growth of the QDs and also nearly avoids the light propagation through the highly-dislocated substrate/nitride interface..

Slab modal guiding is significantly reduced when ranging the ridge etching depth from 250 nm to 550 nm being 350 nm the optimum value for nonlinear processes since it presents the lowest theoretical mode effective area (~1.6 µm^2) in the range under study (see ref. [19]). The cross-section and normalized modal amplitude color map for the GaN/AlN QDs WG is shown in Fig. 3(a).

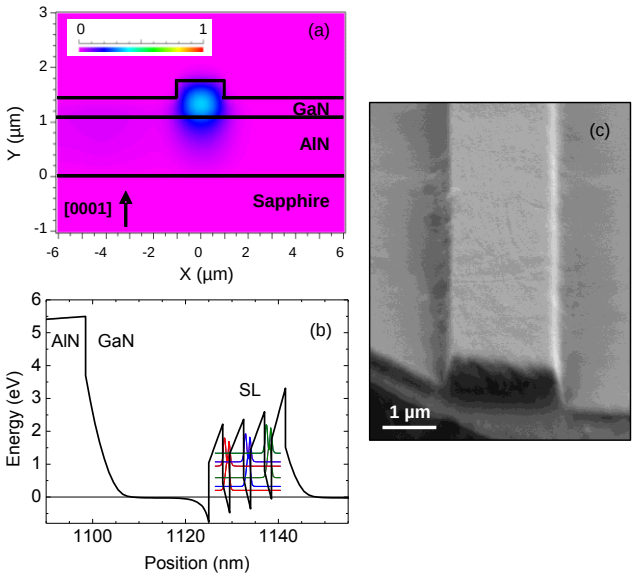

Figure 3 (a) Simulated cross-section and normalized modal amplitude color map at the output facet of a 2-mm-long and 2-µm-wide GaN/AlN QD-based WG. (b) Calculation of the conduction band diagram and electronic levels in the active region. (c) FE-SEM image of the 2-µm-wide and 350-nm-deep WG before the facet polishing procedure.

The active media was design to be 3 periods of 1–1.5-nm-high GaN QDs and 3-nm-thick AlN barriers in order to ensure a measurable transmitance in 2-mm-long WGs. The dimensions of the active nanostructures were calculated to tune the intraband transition to 1.55 µm (see ref. [26]). Figure 3(b) presents the conduction band profile together with the electronic levels in the active region.

Previously to the growth of the QDs nanostructures, a ~25-nm-thick GaN buffer layer is synthesized in order to ensure the electronic population in the first confined level, making efficient the intraband transition [see inset of Fig. 3(b)].

4.1.2 Waveguide fabrication The sample was synthesized by plasma-assisted MBE. The details about the growth of the GaN guiding layer and the QDs can be found elsewhere [19][26]. The 2-µm-wide WGs were firstly defined by UV lithography and etched by induced coupled plasma reactive-ion etching (ICP-RIE) using $SiCl_4$ and N_2 plasma. Finally, WGs facets were mechanically polished. Figure 3(c) shows the field emission scanning electron microscopy (FESEM) image of the GaN/AlN WG pointing to the high-quality etching process.

4.1.3 Optical measurements Figure 4(a) shows the transmittance for TE- and TM-polarized light as a function of the WG length. Total coupling losses of 22 dB and 26 dB are obtained for TE- and TM-polarized light, respectively. These values are quite large since the optical launching area of the WG (2 µm wide and 350 nm deep) is smaller than the optical mode coming out from the optical lensed fiber, with a diameter of 2.5 µm. Besides, the 4 dB difference between coupling losses for TE- and TM-polarized light is due to the asymmetry of the WG geometry (ridge width > ridge height)

Propagation losses of 11 dB/mm and 39 dB/mm are extracted for TE- and TM-polarized light, respectively. The high value obtained for the TM polarization confirms the QD intraband absorption at telecom wavelength.

Figures 4(b) and 4(c) depict the optical TE and TM transmittance and the transmittance increase for TM-polarized light, respectively, as a function of the input pulse energy for a the 2-µm-wide GaN/AlN QD-based WG with a length of 1.5 mm. A transmittance increase of 24 dB from low to high input pulse energies is reported for TM-polarized light, and no variation of the transmittance is observed for TE-polarized light.

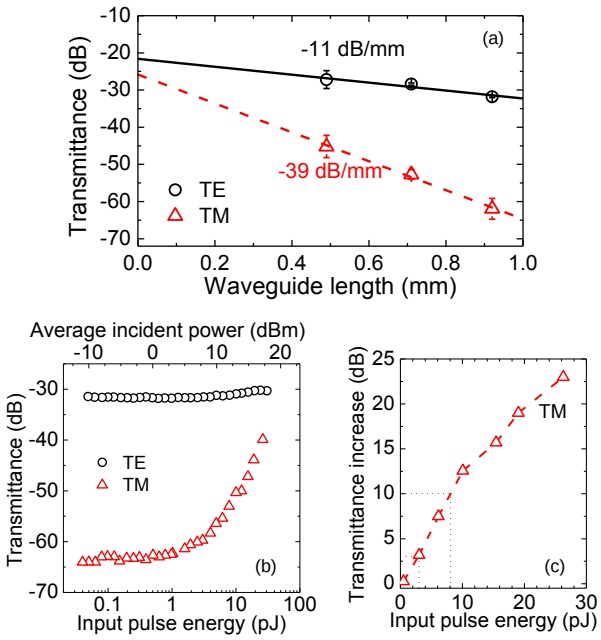

Figure 4 GaN/AlN QD-based WG: (a) Cut-back method; experimental TE-TM transmittance at incident optical power of -12 dBm as a function of the WG length. (b) TE-TM transmittance and (c) TM transmittance increase versus control pulse energy measured in a 1.5-mm-long WG.

The nonlinear efficiency can be evaluated by considering the input pulse energy required to reach the +3 dB of transmittance change. In this case, the input pulse energy required for 3 dB (10 dB) absorption saturation is as low as 3 pJ (8 pJ) for 150 fs pulses, assuming the coupling losses formerly estimated. These results confirm GaN/AlN QD-based WGs as efficient saturable absorbers at 1.55 µm.

4.2 Sputtered InN waveguides Nanocrystalline InN deposited by RF sputtering presents high nonlinearities associated with TPA at 1.55 µm, with subpicosecond recovery times [18]. Moreover, RF sputtering is a low-cost thermally-harmless deposition technique. Therefore, the development of WGs based on sputtered InN arises as a potential solution for ultrafast all-optical limiters, which could be used for advanced pulse shaping and device protection [28] in III-nitride-based PICs.

In this section we report the growth, fabrication and optical characterization of WGs based on compact InN material, designed to work as reverse saturable absorbers for all-optical limiting applications at 1.55 µm. Optical loss contrast of 3 dB is obtained for input pulse energies as low as ~1.1 pJ.

4.2.1 InN growth and characterization The InN guiding layer was deposited by RF sputtering on *c*-sapphire taking advantage of its lower refractive index compared to AlN or GaN. Pure N_2 (6N) was used as reactive gas whereas indium was provided by a pure In (4N5) target. The N_2 flux, working pressure, substrate temperature and RF power during deposition were fixed to 14 sccm, 3.5 mTorr, 300 °C and 40 W, respectively. Following these growth conditions, a compact layer morphology is ensured for an InN maximum layer thickness of 350 nm. It should be pointed out that WGs based on compact layers also show a reduction of the Rayleigh scattering losses [21]. Details about the optimized deposition conditions and their influence on the InN material quality are published elsewhere [27].

High-resolution x-ray diffraction (HRXRD) and atomic force microscopy (AFM) measurements were used to assess the structural and morphological quality of the grown 350-nm-thick layer, respectively. The InN film shows a wurtzite crystal structure grown along the *c*-axis, with a ω-scan full width at half maximum of the (0002) x-ray reflection of 2.2º. Figure 5(a) exhibits the AFM image of the compact InN layer which presents a root-mean-squared (rms) surface roughness of 6 nm.

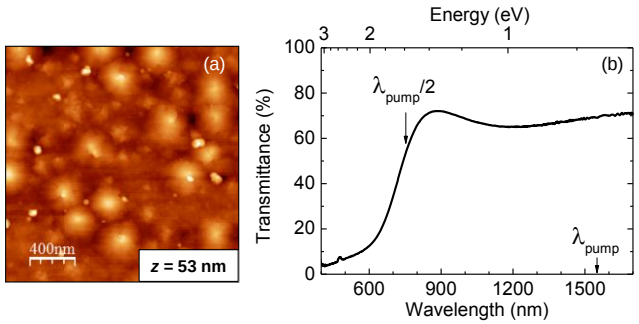

Figure 5 (a) AFM image (2×2 µm^2) and (b) RT linear transmittance spectra of a 350-nm-thick compact InN layer.

Linear transmittance measurements were performed using an optical spectrum analyzer in the visible/near-infrared spectral range at RT. Figure 5(b) shows the linear transmittance spectrum of the analyzed InN film, displaying weak optical absorption at $\lambda_{pump}/2$ (775 nm). The apparent optical bandgap energy and the absorption band edge broadening (ΔE) were evaluated following the procedure described in ref. [29]. The estimated absorption band edge energy E_{abs}~1.77 eV (700 nm) and broadening ΔE~0.13 eV allow close-to-resonant TPA at 1.55 µm.

4.2.1 Waveguide optical design and fabrication Optical calculations considered the InN layer thickness of 350 nm and a ridge width of 2 µm, and the ridge etching depth was varied from 50 nm to 350 nm to ensure single mode propagation along the WG. Results point to an optimum etching depth of 350 nm, since it leads to single mode propagation with the lowest mode effective area (~0.9 µm^2) [see Fig. 6(a)].

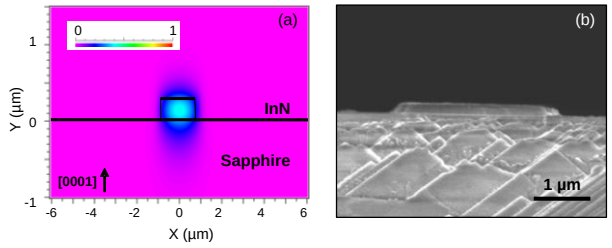

Figure 6 InN WG (2-µm-wide, 350-nm-deep and 2-mm-long): (a) Simulated cross-section and normalized modal amplitude color map at the output facet. (b) FESEM cross-sectional image of the InN WG.

InN WGs were defined by UV lithography and etched down by RF sputtering. Specifically, the sputtering conditions for the etching process were pure Ar (5N) atmosphere, room temperature, 40 W of RF power applied to the substrate and 3.5 mTorr of sputtering pressure. Under these conditions, the etching rate of the InN guiding layer was ~7 nm/min. The WG facets were mechanically polished. Figure 6(b) shows a FESEM cross-sectional image of the InN WG.

4.2.1 Optical waveguide characterization The cut-back method was performed at -2 dBm of incident optical power to estimate both coupling and propagation losses, as illustrated in Fig. 7(a). Total coupling (~50 dB for both polarizations) and propagation losses (8.9 dB/mm and 8.6 dB/mm for TE and TM-polarized light, respectively) were estimated for the InN WG under study. A more significant difference between both polarization responses should be expected because the WG geometrical asymmetry. However, no polarization dependence is observed, probably due to an enhanced Rayleigh scattering in the WG sidewalls defined by the sputtering etching.

Figures 7(b) and 7(c) depict the optical transmittance and the loss increase for TE- and TM-polarized light, respectively, as a function of the input pulse energy for an InN WG with a length of 2.1 mm. A decrease of the optical transmittance occurs at high input pulse energies, reaching a maximum contrast of 6 dB and 4.5 dB for TE- and TM-polarized light, respectively. This polarization-dependent response is due to the intrinsically asymmetry of the hexagonal wurzite InN crystals. TE-polarized light pumps the sample directly onto the basal crystallographic plane of the InN hexagons, exciting the components of the third-order susceptibility tensor responsible of the nonlinear TPA related to this plane. However, TM-polarized light excites the component along the *c*-axis since the electric field vibrates along the hexagon axis [30].

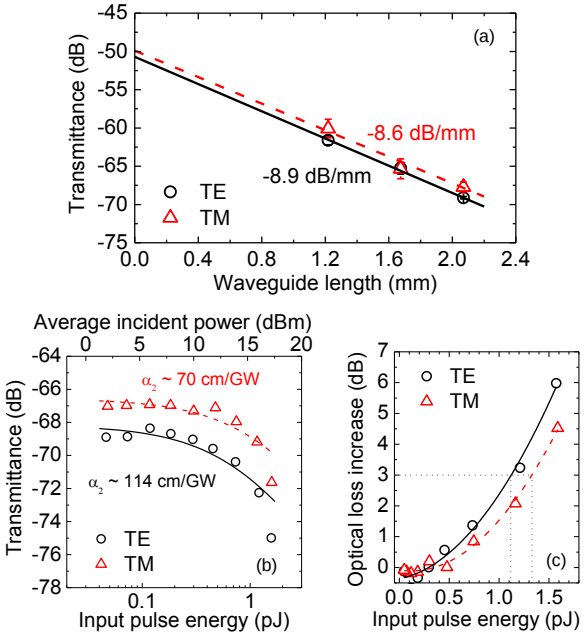

Figure 7 InN WG: (a) Cut-back method; experimental TE-TM transmittance at minimum incident power (-2 dBm) as a function of the WG length. (b) Transmittance and (c) optical loss increase versus control pulse energy for TE- and TM-polarized light measured in a 2.1-mm-long WG. In (b) the lines are fitting curves to Eq. 1 in linear scale.

This reverse saturable absorption effect is attributed to a TPA absorption process. The nonlinear transmittance along the length of the WG (L) can be modeled as a function of the input pulse energy (E_{pulse}) as follows [31]:

$$T_{TPA} = \frac{e^{-\alpha_0 L}}{1+\alpha_2\left(\frac{1-e^{-\alpha_0 L}}{\alpha_0}\right)\frac{E_{pulse}}{A_{eff}\cdot\Delta t}} \qquad (1)$$

with A_{eff} the effective mode area, Δt the temporal pulse width of the input mode, α_0 a parameter related to the WG optical losses, and α_2 the nonlinear absorption coefficient of the active layer. The fit of the experimental data in linear scale to Eq. 1 [lines in Fig. 7(b)] allows the estimation of the parameters such as α_0~75 cm^{-1} for both

polarizations and α_2 = 70±20 cm/GW and 114±30 cm/GW for TM- and TE-polarized light, respectively. These estimated values of α_2 agree with that obtained in InN thick films deposited by RF sputtering [18]. The value of α_2 is larger than those reported for InP, Si(111) and GaAs [32],[33].

At high input pulse energies / intensities (1.6 pJ / 2.7 GW/cm^2), the difference between the experimentally obtained increased absorption and the theoretical value extracted from Eq. 1, indicates the presence of another nonlinear effect with significant strength at these power levels [see Fig. 7(b)]. This additional contribution is attributed to the absorption of free carriers photo-generated by the instantaneous TPA [34].

In terms of nonlinear efficiency, InN WGs require input pulse energies of ~1.1 pJ at 1.55 µm to reach –3 dB of transmittance change for 150 fs pulses, assuming the coupling losses formerly estimated.

4.3 Passive sputtered AlN waveguides A PIC technology requires the development of both active and passive devices, preferably using the same semiconductor family and substrate, to reduce interconnection losses. In this sense, the non-absorptive optical behavior of AlN at 1.55 µm, with a wide band gap of 6.2 eV, which prevents absorption via multiple photons, makes it interesting as optical passive WG within III-nitride-based PICs.

4.3.1 AlN growth and characterization This work focuses on AlN-on-sapphire structures deposited by RF sputtering. AlN guiding layers were deposited by RF sputtering in pure N_2 atmosphere, with an RF power of 150 W applied to the pure Al (5N) target, a substrate temperature of 450 ºC, and a pressure of 3.5 mTorr. Further details about the deposition process (two-step method) and its influence on the AlN material quality are published elsewhere [35]. Typically, these layers show a significantly low rms roughness of ~1.1 nm, and an optical band gap of ~6.0 eV (206 nm). They are highly transparent at 1.55 µm (86% of transmittance).

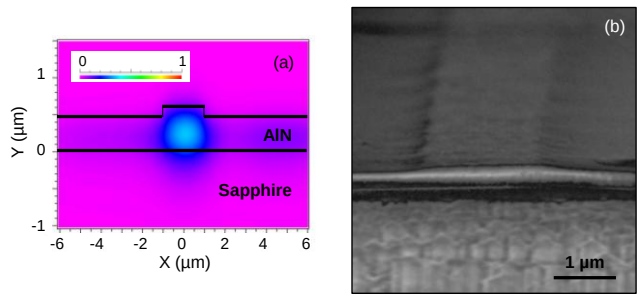

Figure 8 AlN WG (2-µm-wide, 125-nm-deep and 2-mm-long): (a) Simulated cross-section and normalized modal amplitude color map at the output facet. (b) FESEM image of the cross-section and surface view.

4.3.2 Waveguide optical design and fabrication The ridge etching depth of the WGs was determined by optical simulations considering a nominal 600-nm-thick AlN guiding layer with a ridge width of 2 µm to fit with GaN/AlN-based WGs. Single mode propagation was obtained for ridge etching depths below 200 nm and above 500 nm. Considering technological limitations related to the insufficient Al metal mask deposited for the etching process, the final targeted etching depth was 150 nm. Fig. 8(a) shows the scheme of the AlN WG design and the simulated normalized modal amplitude color map at the output facet.

The WGs based on deposited AlN guiding layers were patterned by UV lithography and etched by ICP-RIE using SF_6 and O_2 at RT, reaching an etching depth of ~125 nm. The facets were mechanically polished. Fig. 8(b) shows a FESEM image of the fabricated AlN WG.

4.3.2 Optical waveguide characterization Cut-back measurements were performed [see Fig. 9(a)] showing higher propagation losses for TE polarization (7.1 dB/mm) compared to TM polarization (4.1 dB/mm). This difference can be likely due to diffractive effects along the (x,z)-plane associated with the low-confinement of light along the x-axis and also the influence of the mismatched AlN/sapphire interface on the confined optical mode, which is higher for TE-polarized light, since it vibrates in the plane perpendicular to the growth axis. Optical coupling losses considering both input and output facets are estimated to be 40.1 dB and 41.7 dB for the TE- and TM-polarized light, respectively. This ~2 dB of difference is due to the WG asymmetry. Figure 9(b) depicts the optical transmittance as a function of the input pulse energy. The WG responds linearly for energies up to 4 pJ (average incident power ~15 dBm).

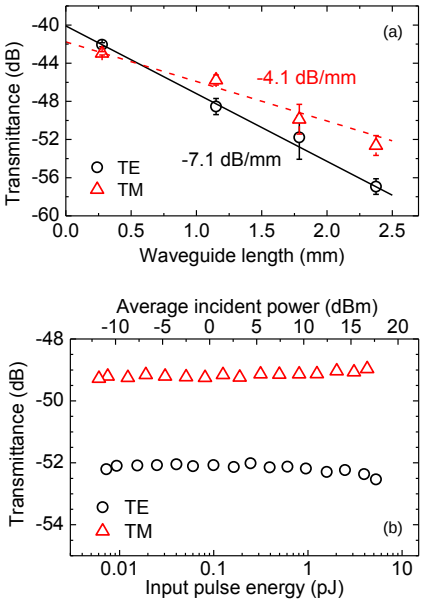

Figure 9 AlN WG: (a) Cut-back method; experimental TE-TM transmittance measured for an incident power of -12 dBm as a function of the WG length. (b) Transmittance versus control pulse energy for TE- and TM-polarized light measured in a 1.8-mm-long WG.

5 Conclusion We have introduced the bases for further implementation of different all-optical functions within a PIC based on III-nitride-based WGs operating at 1.55 μm have been introduced. Active nonlinear devices incorporating GaN/AlN QD heterostructures have demonstrated their capability to act as saturable absorbers reaching a transmittance change of +3 dB for input pulse energies of ~3 pJ with 150-fs pulse width. Besides, sputtered-InN-based WGs present nonlinear behavior via TPA processes reaching a change in transmittance of −3 dB for input pulse energies as low as ~1 pJ. Finally, sputtered-AlN WGs can fulfill the objective of passively interconnecting different active WGs within the PIC. In this way, the implementation of ultrafast all-optical integrated circuits working at data transmission rates ≥1 Tbps per channel could be attained by using the III-nitride semiconductors.

Acknowledgements This work was supported by the Spanish Government projects TEC2012-37958-C02-01 and 02, the Comunidad de Madrid projects S2009/ESP-178 and S2013/MIT-2790, the University of Alcalá project CCG2013/EXP-052, the EU Marie Curie IEF 'SolarIn' (#331745) project, and the EU ERC-StG 'TeraGaN' (#278428) project. The authors would like to acknowledge E. Barrios for lithography process assistance.

References

[1] O. Wada, New J. Phys. **6**, 183 (2004).
[2] Christopher R. Doerr, IEICE Trans. Electron. **E96-C**, 950 (2013).
[3] V. Lal *et al.*, in: IEEE Proc. Photonics Society Summer Topical Meeting Series, (2011) pp. 117–118.
[4] L. Liao, A. Liu, D. Rubin, J. Basak, Y. Chetrit, H. Nguyen, R. Cohen, N. Izhaky and M. Paniccia, Electron. Lett. **43**, 1196 (2007).
[5] J. Pleumeekers *et al.*, in: CS MANTECH Conference, New Orleans, Louisiana, USA, May 13–16 (2013).
[6] J. Wu, J. Appl. Phys. **106**, 011101 (2009).
[7] M. Beeler, E. Trichas, and E. Monroy, Semicond. Sci. Technol. **28**, 074022 (2013).
[8] M. Tchernycheva, L. Nevou, L. Doyennette, F.H. Julien, E. Warde, F. Guillot, E. Monroy, E. Bellet-Amalric, T. Remmele, and M. Albrecht, Phys. Rev. B **73**, 125347 (2006).
[9] S. Valdueza-Felip, F.B. Naranjo, M. González-Herráez, H. Fernández, J. Solís, F. Guillot, E. Monroy, L. Nevou, M. Tchernycheva, and F. Julien, IEEE Photon. Technol. Lett. **20**, 1366 (2008).
[10] N. Suzuki and N. Iizuka, Jpn. J. Appl. Phys. **36**(Part 2), 1006 (1997).
[11] N. Iizuka, K. Kaneko, N. Suzuki, T. Asano, S. Noda, and O. Wada, Appl. Phys. Lett. **7**, 648 (2000).
[12] J. Hamazaki, S. Matsui, H. Kunugita, K. Ema, H. Kanazawa, T. Tachibana, A. Kikuchi, and K. Kishino, Appl. Phys. Lett. **84**, 1102 (2004).
[13] J.D. Heber, C. Gmachl, H.M. Ng, and A.Y. Cho, Appl. Phys. Lett. **81**, 1237 (2002).
[14] R. Rapaport, G. Chen, O. Mitrofanov, C. Gmachl, H.M. Ng, and S.N. Chu, Appl. Phys. Lett. **83**, 263 (2003).
[15] F.B. Naranjo, M. González-Herráez, H. Fernández, J. Solís, and E. Monroy, Appl. Phys. Lett. **90**, 091903 (2007).
[16] F.B. Naranjo, P. Kandaswamy, S. Valdueza-Felip, V. Calvo, M. González-Herráez, S. Martín-López, P. Corredera, J.A. Méndez, G. Mutta, B. Lacroix, P. Ruterana, and E. Monroy, Appl. Phys. Lett. **98**, 031902 (2011).
[17] S. Valdueza-Felip, L. Rigutti, F.B. Naranjo, P. Ruterana, J. Mangeney, F. Julien, M. González-Herráez, and E. Monroy, Appl. Phys. Lett. **101**, 062109 (2012).
[18] S. Valdueza-Felip, L. Monteagudo-Lerma, J. Mangeney, M. González-Herráez, F.H. Julien, and F.B. Naranjo, IEEE Photon. Technol. Lett. **24**, 1998 (2012).
[19] L. Monteagudo-Lerma, S. Valdueza-Felip, F.B. Naranjo, P. Corredera, L. Rapenne, E. Sarigiannidou, G. Strasser, E. Monroy, and M. González-Herráez, Opt. Express **21**, 27578 (2013).
[20] L. Monteagudo-Lerma, F.B. Naranjo, M. Jiménez-Rodríguez, P.A. Postigo, E. Barrios, P. Corredera, and M. González-Herráez, IEEE Photon. Technol. Lett. **27**, 1857 (2015).
[21] S. Birner, T. Zibold, T. Andlauer, T. Kubis, M. Sabathil, A. Trellakis, and P. Vogl, IEEE T. Electron Dev. **54**, 2137 (2007).
[22] P.K. Kandaswamy, F. Guillot, E. Bellet-Amalric, E. Monroy, L. Nevou, M. Tchernycheva, A. Michon, F.H. Julien, E. Baumann, F.R. Giorgetta, D. Hofstetter, T. Remmele, M. Albrecht, S. Birner, and L.S. Dang, J. Appl. Phys. **104**, 093501 (2008).
[23] R.G. Hunsperger, Integrated optics: theory and technology. (Springer-Verlag, Berlin, 1995), p. 87.
[24] S. Noda, T. Yamashita, M. Ohya, Y. Muromoto, and A. Sasaki, IEEE J. Quantum Elect. **29**, 1640 (1993).
[25] Y. Li, A. Bhattacharyya, C. Thomidis, T.D. Moustakas, and R. Paiella, Opt. Express, **15**, 17922 (2007).
[26] F. Guillot, E. Bellet-Amalric, E. Monroy, M. Tchernycheva, L. Nevou, L. Doyennette, F. H. Julien, L. S. Dang, T. Remmele, M. Albrecht, T. Shibata, and M. Tanaka, J. Appl. Phys. **100**, 044326 (2006).
[27] L. Monteagudo-Lerma, S. Valdueza-Felip, A. Núñez-Cascajero, A. Ruiz, M. González-Herráez, E. Monroy, and F.B. Naranjo, J. Cryst. Growth (under review).
[28] M. Bass, in: Handbook of Optics: Fiber optics and nonlinear optics (McGraw-Hill, New York, 2000), chap. 19.
[29] F.B. Naranjo, M.A. Sánchez-García, F. Calle and E. Calleja, Appl. Phys. Lett. **80**, 231 (2002).
[30] K. Wang, J. Zhou, L. Yuan, Y. Tao, J. Chen, P. Lu, and Z. L. Wang, Nano Lett. **12**, 833 (2012).
[31] J.S. Aitchison, D.C. Hutchings, J.U. Kang, G.I. Stegeman, and A. Villeneuve, IEEE J. Quantum Electron. **33**, 341 (1997).
[32] D. Vignaud, J. Lampin, and F. Mollot, Appl. Phys. Lett. **85**, 239 (2004).

[33] M. Dinu, F. Quochi, and H. García, Appl. Phys. Lett. **82**, 2954 (2003).
[34] A.C. Turner-Foster, M.A. Foster, J.S. Levy, C.B. Poitras, R. Salem, A.L. Gaeta, and M. Lipson, Opt. Express **18**, 3582 (2010).
[35] L. Monteagudo-Lerma, S. Valdueza-Felip, A. Núñez-Cascajero, M. González-Herráez, E. Monroy and F.B. Naranjo, Thin Solid Films, **545**, 149 (2013).